Research article

Thermohydraulic analysis of nanofluid flow in tubular heat exchangers with multi-blade turbulators: The adverse effects

Ali Mohadjer [a], Mohammad Hasan Nobakhti [b,*], Alireza Nezamabadi [a], Seyed Soheil Mousavi Ajarostaghi [c]

[a] Department of Mechanical Engineering, Arak Branch, Islamic Azad University, Arak, Iran
[b] Department of Mechanical Engineering, Science and Research Branch, Islamic Azad University, Tehran, Iran
[c] Mechanical Engineering Department, Babol Noshirvani University of Technology (BNUT), Babol, Iran

ABSTRACT

Based on the significance of heat transfer in tubular flows, various methods of heat transfer enhancement have been developed by scholars. The use of turbulator inserts like twisted tapes is widely discussed and suggested by researchers, and many studies have concentrated on the positive influence of these devices. However, the question is whether these devices always positively impact heat transfer and fluid flow. In this study, efforts were made to find possible adverse impacts of using twisted tapes on the average Nusselt number (Nu), friction factor (f), flow behavior, and performance evaluation criterion (PEC) of water-titania nanofluid. Three-dimensional (3D) numerical methods were used to assess a combination of three different configurations of 156 cases with/without turbulators with different numbers of blades and pitch ratios (PR). Results suggest that at Reynolds number (Re) = 4000, 6000, and 8000, only 25 %, 25 %, and 22.9 % of the examined cases led to PEC values over 1. Based on the results, while twisted tapes raised the Nu by up to 65.1 %, the f can be increased by up to more than six times. Furthermore, streamlines and velocity magnitude contours were employed to discuss the fluid flow behavior in the presence of the turbulators. According to the findings, while with the best turbulator, the PEC value was increased by only 6.3 %, some of the turbulators reduced this parameter by up to 11.8 %, which is more severe. The worst performance was observed with the Case C (three-bladed) turbulator at a PR value of 11, which reduced the PEC by 11.8 %.

1. Introduction

In the realm of renewable energies like wind and solar power [1,2], the efficacy of harnessing these sources lies in optimizing energy conversion processes. Improving heat exchangers (HXs) becomes paramount, as they play a pivotal role in facilitating efficient thermal management within renewable systems [3]. Enhanced heat transfer (HT) capabilities not only bolster the overall performance of these technologies but also contribute significantly to the advancement of sustainable energy solutions, ensuring a greener and more resilient future [4]. The efficiency of industrial HXs has been improved over the years by applying various methods, such as using fins [5–7], porous media, nanofluids, and swirling flow devices [8]. The swirling flow of fluid is created by embedding a suitable swirl flow device in the circular tube. To increase the performance of HXs, various shapes of such turbulators were suggested by researchers

---

[8–10]. Stalin et al. [11] investigated the effectiveness of cinque-faced rib roughening in improving the efficiency of solar air heaters (SAHs) by introducing a novel design called the cinque-faced rib-roughened triangular channel SAH. Their study aimed to analyze the performance of this design considering parameters such as relative roughness pitch and height. The findings revealed remarkable efficiency of up to 80.7 % under optimal roughness parameters, showcasing the potential of this innovative design in enhancing solar energy utilization. Singh et al. [12] investigated the impact of various obstacle shapes, including Isosceles trapezoid and triangular with curved apex, on *Nu* and *f* in SAH ducts. The study revealed maximum enhancements in *Nu* and *f* with rectangular with curved edges obstacles in a staggered configuration, showing an average enhancement factor of 4.37. Additionally, they evaluated the thermo-hydraulic performance parameter. Alam et al. [13] investigated the thermo-hydraulic performance of small conical ribs on an SAH absorber plate using exergy analysis. They aimed to optimize the rib design by simultaneously considering thermal and hydraulic performance. The study revealed that the combination specific rib parameters, such as relative rib height and pitch, resulted in the highest exergy efficiency. Additionally, they highlighted the significant impact of solar insolation and Re on exergy efficiency, emphasizing the importance of considering surface roughness effects in SAH design. Kumar et al. [14] investigated the enhancement of thermal efficiency in parabolic trough solar collectors (PTSCs) by utilizing innovative coolant nanofluids (NFs) and a reconfigured receiver tube with oval ribbing. They analyzed the thermal and hydraulic performance of the modified PTSC across various parameters. Their findings revealed that the incorporation of oval ribbed receiver tubes significantly improved heat transfer within the system. Dash et al. [15] explored the impact of cylindrical ribs with variable sector angles on heat transfer in microchannel passages. Their study focused on analyzing the *Nu*, *f*, and performance values in the Re range of 100–900. They found that changes in rib sector angles influenced *Nu* and *f* with the highest enhancement observed at a sector angle of 80°. Ishaque et al. [16] explored the impact of HX design on heat pump performance under partial load conditions. They conducted numerical analysis and achieved a maximum seasonal performance enhancement of 7.07 %. Their findings highlighted the importance of air-side flow uniformity and suggested potential energy savings through optimized HX configurations. Nazir et al. [17] delved into the hydrothermal performance of PTSC concentrating systems and focused on the absorber tube. They systematically reviewed various turbulators employed in PTSCs, considering Nusselt number (*Nu*), mean friction factor (*f*), and thermal–hydraulic behavior. Introducing a novel PTSC with a combination of corrugated channels and obstacles, they demonstrated enhanced thermal-hydraulic performance compared to individual turbulators. The study highlighted the effectiveness of using specific geometries, such as ribbed absorber tubes and concentric rod inserts, providing valuable insights for optimizing PTSC designs. Chupradit et al. [18] explored the use of HXs with unique specifications in the food and automotive industries. Employing Cu-based nanoparticles and Chloro-difluoromethane (R22) as NFs, they simulated HT in a turbulator using Fluent Software. The study focused on varying variables in a shell tube HX, including twist pitch ratio and diameter ratio. The results indicated significant increases in *Nu* with higher diameter ratios, especially at elevated Reynolds numbers. Furthermore, they observed enhanced HT in turbulators at higher Reynolds numbers and increased torsion pitch ratios. Esmaeili et al. [19] investigated the enhancement of thermal performance in parabolic solar collectors (PTCs) through the simultaneous use of turbulators and NFs as the working fluid. Utilizing three-dimensional numerical simulations, the study explored the impact of different turbulator types and hybrid nanoparticles on HT and entropy generation in a PTC absorber tube. The introduction of conical helical gear rings as turbulators resulted in a 35.7 % increase in HT and a 32.8 % reduction in total entropy generation. The study demonstrated that turbulator insertion significantly improves HT coefficients, with the Bejan number consistently indicating the prevalence of thermal entropy generation in all cases. Xiong et al. [20] conducted a comprehensive numerical simulation on double-pipe HXs with conical and fusiform turbulators. Involving 21 configurations and considering various tube shapes and Reynolds numbers, the study revealed that circular inner pipes resulted in the maximum convective HT coefficient. The optimal configuration was identified as the tube with circular inner pipes and 12 mm fusiform turbulators. The findings emphasized the significance of turbulator diameter in enhancing HT and highlighted the trade-off between HX performance and pressure drop. Chaurasiya et al. [21] employed numerical simulations to explore corrugation effects on inner tube surfaces in a double-pipe HX. They examined internally and externally corrugated tubes at various helix angles. Results favored externally corrugated tubes, especially at a helix angle value of 15°, showing enhanced efficiency. They emphasized that further investigations are needed on the corrugation's impact, especially regarding helix angle variations.

Twisted tapes (TTs) are known as one of the common turbulators because their design and construction are very simple. They are widely employed for rotating the fluid and escalating the turbulence level within the tubes or channels. By making use of TTs as turbulators, the HT level is improved, which can result in a dramatic reduction in the size of the equipment. Different shapes of HXs with various TTs as turbulators were studied by many researchers [22–24]. Heeraman et al. [25] explored *Nu* and *f* properties in a double-pipe HX with TT inserts with dimple configurations. They investigated the effects of various dimple sizes and dimple diameter-to-depth ratios on these properties. Their findings revealed that TT inserts with dimples significantly enhance heat transfer rate and friction factor compared to plain tube arrangements, particularly beyond a certain Reynolds number threshold. Singh et al. [26] investigated the impact of toothed V-cut TT inserts on *Nu*, *f*, and performance properties in a double-pipe HX. Their experiments revealed that incorporating teeth on the v-cut TTs enhances results in better performance, particularly at higher Reynolds numbers, owing to secondary vortex flow generation. Additionally, the toothed v-cut inserts showed a superior balance between *Nu* and *f* properties. Sundar [27] investigated the HT characteristics of nanodiamond-Fe_3O_4/water hybrid NF in a tube with TT inserts. Experimental evaluations under turbulent flow conditions revealed that the NF exhibited significant enhancements in *Nu* and exergy efficiency compared to plain water tubes, particularly with TT inserts. The use of 0.2 % volume loading of NF, along with a TT insert of 5, showed remarkable improvements in thermal entropy generation reduction (48.58 %) and frictional entropy generation increase (74.81 %). The study emphasized the promising potential of NFs with TT inserts for enhancing HT in HX tubes. Samutpraphut et al. [28] investigated the impact of sawtooth TT (S-TTs) on HT rate, *f*, and aerothermal performance index (API) within a pipe. By introducing intermittent flowing disturbance and swirling flow, the S-TTs demonstrated enhanced HT rates and higher *f* compared to

typical TTs. The optimum API of 1.33 was achieved with the S-TT featuring a 70° sawtooth angle. The study emphasizes the potential of S-TTs, outperforming TT and plain tubes in *Nu*. Feng et al. [29] investigated the HT enhancement in mini-channels using combined inserts of TT and wire coil. The study explored various configurations and found that the mini-channel with a full-length combination of these devices demonstrated the maximum HT rate, while the mini-channel with wire coil alone exhibited the highest overall thermal performance. The findings suggested that the combined structure effectively promoted flow mixing and HT, with the best overall thermal performance observed at different mass flow rates.

In this brief literature review, it was aimed to illuminate the advancements in the field of turbulators and their impact on heat transfer and pressure drop. Previous studies have frequently demonstrated a remarkable augmentation in heat transfer rates through the implementation of turbulators. However, an essential question arises: do turbulators consistently yield favorable effects on heat transfer and fluid flow? This study endeavors to explore potential adverse consequences associated with the use of turbulators on Nu, f, flow behavior, and performance evaluation criterion (*PEC*) of water-titania nanofluid. Employing numerical methods, a comprehensive analysis was conducted across different configurations comprising 156 cases with and without turbulators featuring varying numbers of blades (Case A = 1, Case B = 2, and Case C = 3) and pitch ratios (*PR* = 44, 22, 15, and 11, equivalent to the twist angles of 2π, 4π, 6π and 8π, respectively) at different Re number in the turbulent flow regime (Re = 4000, 6000, and 8000) of titania-water nanofluid with various nanofluid concentrations ($\varphi = 0.01$, 0.02, and 0.03). Unlike most previous studies, which were based on step-by-step optimization, and set the determined and optimized variables constant for the next stages, the simulations were done for the cases with all of these variables, providing an extensive database. Additionally, the study utilized streamlines and velocity magnitude contours to elucidate the fluid flow behavior in the presence of turbulators. By addressing these complexities, the outcomes of this research endeavor aim to provide valuable insights to guide future studies and inform decision-making processes concerning the design and application of turbulators in heat transfer systems.

2. Problem definition and boundary conditions

The heat transfer and flow behavior of nanofluid in a tube equipped with a turbulator are numerically investigated in this article. For this purpose, tubes with lengths and diameters of 0.6 m and 0.00457 m were created in computer-aid design (CAD) software. Since not considering an inlet and outlet zone can lead to errors such as reverse flow in the numerical model, which can negatively influence the accuracy of the setup [30], the tubes were divided into three sections, each with a length of 0.2 m. The reason for considering these two sections before and after the test section (with heated wall) is to eliminate the effects of inlet and outlet conditions on the obtained results. It is important to note that the TTs are located in the middle section of the tube. Fig. 1 (a) shows the tube with different types of turbulators. The cross-section of the turbulator in Case A is a rectangle with a length and width of 0.003 m and 0.0004 m, respectively. In Case B and Case C, the cross sections of turbulators are obtained by connecting two and three rectangles to form a cross or semi-cross shape. Also, the TiO$_2$–H$_2$O nanofluid, the thermophysical characteristics of which are presented in Table 1, is chosen as the working fluid in this study.

The sides of the first and third sections of the tube are insulated; however, a constant heat flux is considered on the side of the tube's middle part, where the turbulators are located. A velocity inlet condition is imposed on the inlet boundary, and an outflow condition is selected for the outlet. The turbulators are created by twisting the tapes around the x-axis. The TTs are twisted with various angles along the tube to create a rotational flow in the fluid. Fig. 1 (b) shows the turbulators from the defined cases. It is necessary to mention that while the twist angles in this figure are 8π, the twisted angles of 2π, 4π, 6π and 8π are also examined for each case. The pitch ratio (*PR*) is known as the ratio of the length of twisted pitch (*p*) to the diameter of the pipe. For the twisted angles of 2π, 4π, 6π and 8π, *PR* is calculated to be 44, 22, 15, and 11, respectively.
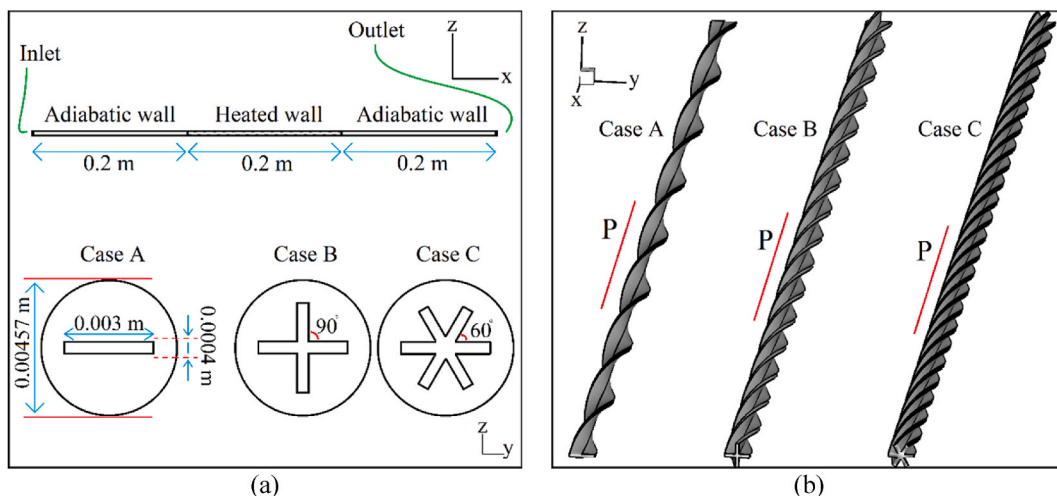

Fig. 1. Tubes with different turbulators. (a) The lateral view of tubes, and (b) the 3D view of turbulators.

Table 1
The thermophysical properties of the materials involved in simulations [31].

Materials	Specific Thermal Capacity [J/kg.K]	Density [kg/m³]	Viscosity [Pa.s]	Thermal Conductivity [W/m. K]
Water	4179	997.1	0.00089	0.605
TiO$_2$	692	4230	–	8.4

3. Governing equations and numerical procedure

Heat transfer and the behavior of nanofluid flow in a pipe with different turbulators are studied by solving the continuity, momentum, and energy equations [32–34]. Based on previous studies [35,36], for modeling turbulence, the Renormalized Group (RNG) k-ε turbulence model is adopted for the simulations, as this approach has a suitable accuracy for considering the effects of swirling flow on turbulence [37]. The RNG k-ε model was introduced to enhance the efficacy of the standard K-ε model, particularly for swirling turbulent flow prediction.

$$\frac{\partial}{\partial x_i}\left(\rho_{nf}\overline{u_i}\right) = 0 \tag{1}$$

$$\frac{\partial}{\partial x_j}\left[\rho_{nf}\overline{u_i u_j} + p\delta_{ij} - \mu_{nf}\left(\frac{\partial \overline{u_i}}{\partial x_j} + \frac{\partial \overline{u_j}}{\partial x_i} - \frac{2}{3}\frac{\partial \overline{u_l}}{\partial x_l}\delta_{ij}\right)\right] + \frac{\partial}{\partial x_j}\left(\rho_{nf}\overline{u_i' u_j'}\right) = 0 \tag{2}$$

$$\frac{\partial}{\partial x_i}\left(\rho_{nf}\overline{u_i}C_{nf}T\right) = \frac{\partial}{\partial x_i}\left(K_{nf}\frac{\partial T}{\partial x_i}\right) \tag{3}$$

$$\frac{\partial(\rho_{nf}k u_i)}{\partial x_i} = \frac{\partial}{\partial x_j}\left(\alpha_k \mu_{eff}\frac{\partial k}{\partial x_i}\right) + G_k + G_b - \rho_{nf}\varepsilon + S_k \tag{4}$$

$$\frac{\partial(\rho_{nf}\varepsilon u_i)}{\partial x_i} = \frac{\partial}{\partial x_j}\left(\alpha_\varepsilon \mu_{eff}\frac{\partial \varepsilon}{\partial x_j}\right) + C_{1\varepsilon}\frac{\varepsilon}{k}(G_k + C_{3\varepsilon}G_b) - C_{2\varepsilon}\rho_{nf}\frac{\varepsilon^2}{k} + S_\varepsilon \tag{5}$$

where, u_i and u_j are the velocities in the x_i and x_j directions. T is the temperature of the nanofluid. k and ε are the kinetic energy of turbulence and the dissipation rate of the kinetic energy of turbulence. G_k and G_b are the generation of kinetic energy of turbulence due to the velocity gradient and buoyancy, respectively. $C_{1\varepsilon}$, $C_{2\varepsilon}$ and $C_{3\varepsilon}$ are constant.

The effective parameters of the employed nanofluid, such as density (ρ_{nf}), heat capacity (C_{nf}), and thermal conductivity (k_{nf}) are defined in the following forms [38]:

$$\rho_{nf} = (1-\varphi)\rho_f + \varphi\rho_p \tag{6}$$

$$C_{nf} = \frac{(1-\varphi)\rho_f C_f + \varphi\rho_p C_p}{\rho_{nf}} \tag{7}$$

$$k_{nf} = \frac{k_f\left(k_p + 2k_f - 2\varphi(k_f - k_p)\right)}{\left(k_p + 2k_f + 2\varphi(k_f - k_p)\right)} \tag{8}$$

Moreover, the nanofluid's viscosity is expressed by the following correlation [39]:

$$\mu_{nf} = \frac{\mu_f}{1 - 34.87\left(\frac{d_p}{d_f}\right)^{-0.3}\varphi^{1.03}} \tag{9}$$

The previous parameter is a function of nanoparticle diameter (d_p), which was considered 25 nm [40], nanofluid concentration, and d_f, which is defined as follows:

$$d_f = \left(\frac{6M_m}{N\pi\rho_f}\right)^{1/3} \tag{10}$$

The effective parameters are then substituted in Eqs. (1)–(5). The correlations are numerically solved with ANSYS Fluent 19.1. The Nu, f, and PEC values are employed to indicate the performance of the HX and are defined as follows:

$$Nu = \frac{\left(\frac{q''}{(T_w - T_m)}\right).D}{k} \tag{11}$$

$$f = \frac{\Delta p}{\frac{\rho u^2}{2} \frac{L}{D}} \quad (12)$$

$$PEC = \frac{\frac{Nu}{Nu_0}}{\left(\frac{f}{f_0}\right)^{1/3}} \quad (13)$$

Regarding the solution method, it should be noted that the second-order upwind scheme is applied to discretize the equations, while The SIMPLE algorithm is chosen to model the pressure-velocity coupling.

4. Validation and grid sensitivity tests

To assess the accuracy of this study, a tube fitted with a two-channel TT insert and constant wall heat flux from the experimental work of Eiamsa-ard and Promvonge [41] was chosen. The inner diameter of the tube was 47 mm, with a thickness and length of 1.5 mm and 1250 mm. To validate both the hydraulic and thermal aspects of the numerical simulation, the validation process was done by analyzing the average Nu and f values within the turbulent Re range of 5000–20000. The result is illustrated in Fig. 2. As can be observed, the numerical method predicts the pattern of changes, and the maximum deviation of the Nu and f are 5.8 and 3.2 %.

Due to the complex nature of tube geometries with turbulator inserts, for all of the cases, an unstructured grid network was generated over the entire computational domain. To be able to better examine the flow and heat transfer in delicate areas, the computational cells located in the regions near the turbulator and wall of the pipe were chosen to be finer. Therefore, the test section where the evaluations were conducted, had more precise mesh sizing compared to the inlet and outlet zones, which were solely added to eliminate the inlet and outlet effects.

To select the sizing setting of the mesh network, Case C with $PR = 44$ was selected as the reference. Grid independence tests were carried out using setups with 435000, 1127000, 1820000, 2463000, and 3176000 cells. The results of the average Nu with each of these setups, as well as their relative difference, have been presented in Fig. 3a. As it can be noticed from these plots, the setup with 2463000 cells has a relative difference of less than 0.13 %; thus, since this option provides the best balance between the accuracy and computational time, it has been selected for this case. The grid network for this case can be observed in Fig. 3b. It is noteworthy that the configurations of this case have been extended to other cases as well.

5. Results and discussions

In this section, the influence of TTs on the changes in thermal and hydraulic behavior of the tubular fluid flow will be discussed. First, a plain tube will be selected as the benchmark case with different NP concentrations, then different TT inserts with various numbers of blades and PRs will be tested at Re = 4000–6000, and their effects on the $Nu, f,$ flow behavior, and the PEC will be extensively discussed.
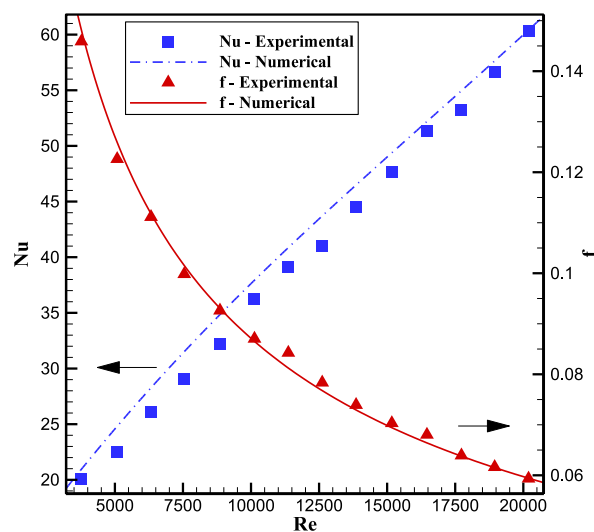

Fig. 2. Comparison of the acquired numerical values with the experimental values of Eiamsa-ard and Promvonge [41]. The red line and blue line indicate the friction factor and Nusselt number values, respectively. (For interpretation of the references to colour in this figure legend, the reader is referred to the Web version of this article.)
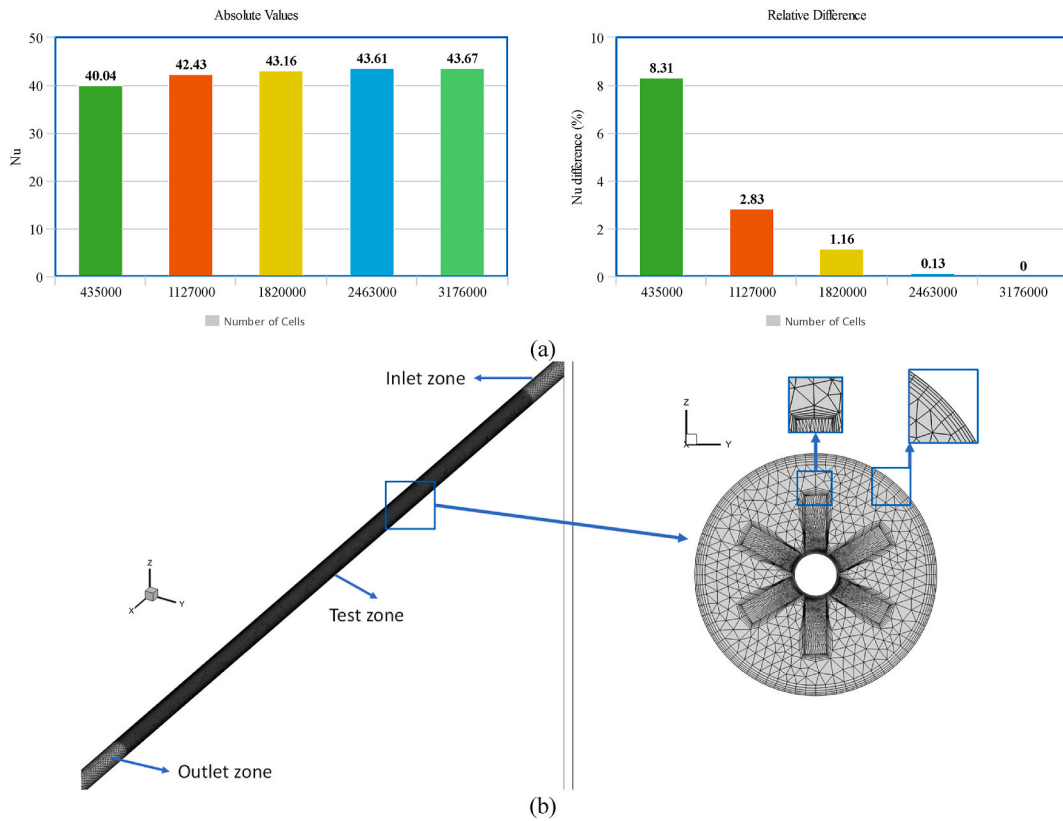
Fig. 3. (a) Grid independence tests, and (b) the generated grid for one of the cases.

5.1. Plain tube (base model)

In a plain tube without a turbulator, the variations of *Nu* and *f* with various nanofluid concentrations and at different Re values are shown in Fig. 4. For this case, the variations in these values show that by raising the *Re*, the *Nu* values are increased, while *f* values are in a downward trend. The obtained results also reveal that with the growth of the nanoparticle concentration, the *Nu* is slightly augmented, while the increment in *f* values seems more severe.
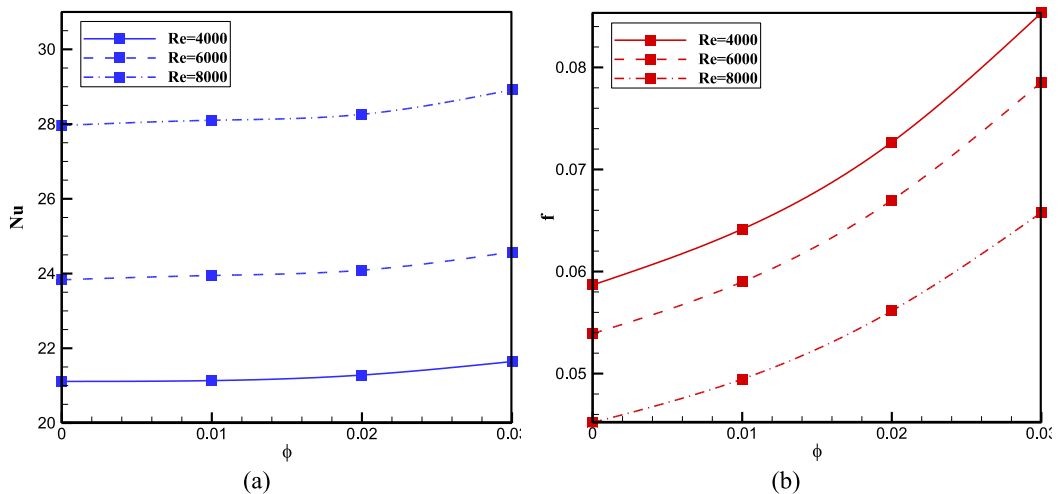

Fig. 4. Variations of (a) *Nu* and (b) *f* with various nanofluid concentrations and Re values for the plain tube without a turbulator.

5.2. The impact of turbulators on the average Nu number

To evaluate the influence of TT insertion in the tubes, simulations were also carried out for the tubes with Case A, B, and C turbulators, with *PR* values of 44, 22, 15, and 11 at Re = 4000, 6000, and 8000. The variation of *Nu* and *Nu/Nu₀* ratios at various nanofluid concentrations for different cases and different *PR* values at Re = 4000 is shown in Fig. 5a. Looking at *Nu/Nu₀* ratios shows
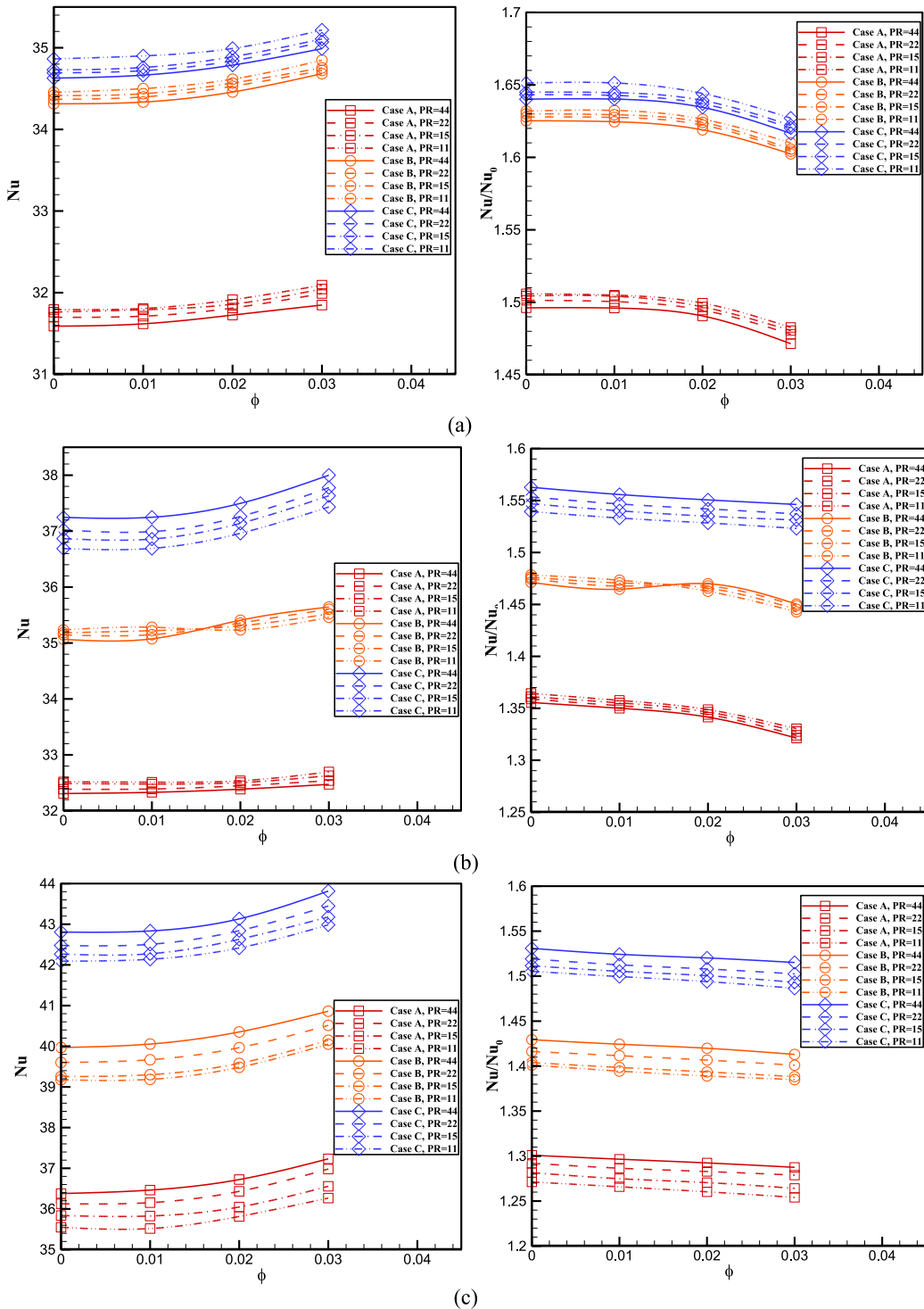

Fig. 5. Variation of *Nu* and *Nu/Nu₀* for (a) Re = 4000, (b) Re = 6000, and (c) Re = 8000.

that the insertion of turbulators in the tube leads to the increase in the value of *Nu* with ratios between 1.651 and 1.471, meaning that at this *Re*, the *Nu* number was increased at least 47.1 % (for Case A turbulator with *PR* = 11) and at maximum 65.1 % (for Case C turbulator with *PR* = 44). The reason can be sought in the alternation of the boundary layer on the tube wall under the effects of the rotational motion of fluid near the walls in the cases with turbulators. The changes in the flow pattern will be later discussed using the streamline and contours. It is found that *Nu* increases with the growth in the number of turbulator blades. Since the flow is guided by the grooves of turbulators, in the cases with a higher number of turbulator blades, a higher portion of the fluid is affected by the TT, and
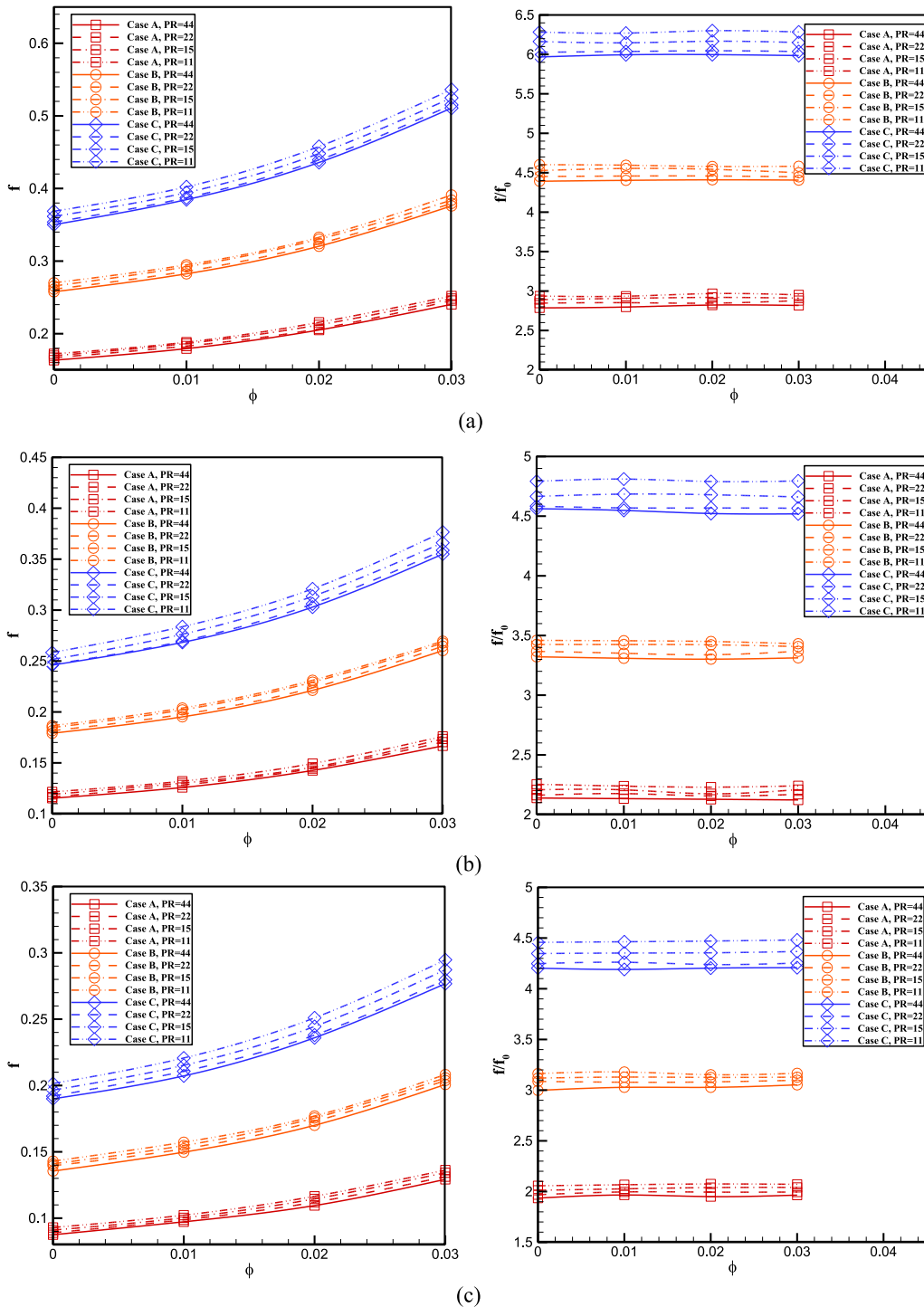

Fig. 6. The *f* and *f/f₀* values for different *PRs* at (a) Re = 4000, (b) 6000, and (c) 8000.

Nu can be expected to increase in these cases. Therefore, the *Nu* for Case C is more than that of Case B, and the *Nu* for Case A is lower than that of Case B. According to Fig. 5a, *Nu* is reduced by the growth in the value of *PR*. In other words, raising the *PR*, which is equivalent to the reduction of the twist angle, weakens the rotational motion of fluid in the vicinity of the hot walls. This seems logical, as with higher *PR* values, the twist angle of TTs is reduced, and since at this *Re*, the flow can follow the twist pattern of the TTs, lower twist angles are associated with less rotational flow and a lower level of turbulence; thus, it offers lower *Nu* numbers. Another critical point is that even though higher NP concentrations are associated with higher *Nu* numbers, the *Nu/Nu$_0$* ratios are reduced as this variable is raised. In other words, at higher NP concentrations, the influence of TTs in raising the *Nu* loses some of its significance.

The effect of turbulators with different pitch ratios on *Nu* and *Nu/Nu$_0$* ratios at the Re = 6000 is shown in Fig. 5b. It can be noticed that based on the *Nu/Nu$_0$* ratios that by inserting the turbulators in the tube, the ratios range between 1.562 and 1.321, meaning that at this *Re,* the *Nu* number was increased at least 32.1 % (for Case A turbulator with *PR* = 44) and at maximum 56.2 % (for Case C turbulator with *PR* = 44). As it can be observed, while *Nu* increases with the growth in the number of the turbulator blades (Case C > Case B > Case A) at Re = 6000, this parameter is a complicated function of *PR*. For Case A, *Nu* is a descending function of *PR*; whereas, it is an increasing function of *PR* for Case C. In the tube with the Case B turbulator, *Nu* is an increasing function of *PR* in the lower nanofluid concentrations and a decreasing function of *PR* in the higher nanofluid concentrations. Nevertheless, regardless of the turbulator geometric shape or NP concentration, the presence of TTs, improves the *Nu* number at this Re number, even though the improvement is not as significant as the augmentations at Re = 4000.

The variation of *Nu* at different *PR* and nanofluid concentrations is shown in Fig. 5c for the cases at Re = 8000. As depicted in this figure, the range of the *Nu/Nu$_0$* ratio is between 1.530 and 1.254, which means the improvement in the *Nu* number over the base model (plain tube) was between 53.0 % (for Case C turbulator with *PR* = 44) and 25.4 % (for Case A turbulator with *PR* = 11). By observing the pattern of changes in the *Nu* values, it is evident that the value of *Nu* grows by raising the number of turbulator blades. It means that *Nu* in Case C is more than that in Case B and *Nu* of Case B is more than that of Case A. By increasing the number of TT blades, the flow of fluid is highly affected by the turbulators and the stronger rotational motion of the fluid is created in the tube. The results also reveal that *Nu* increases with the growth in the value of *PR* at the Re = 8000, because, as it will be discussed later using the streamlines, they cannot properly follow the TT profile if the TT has a high twist angle (a low *PR*).
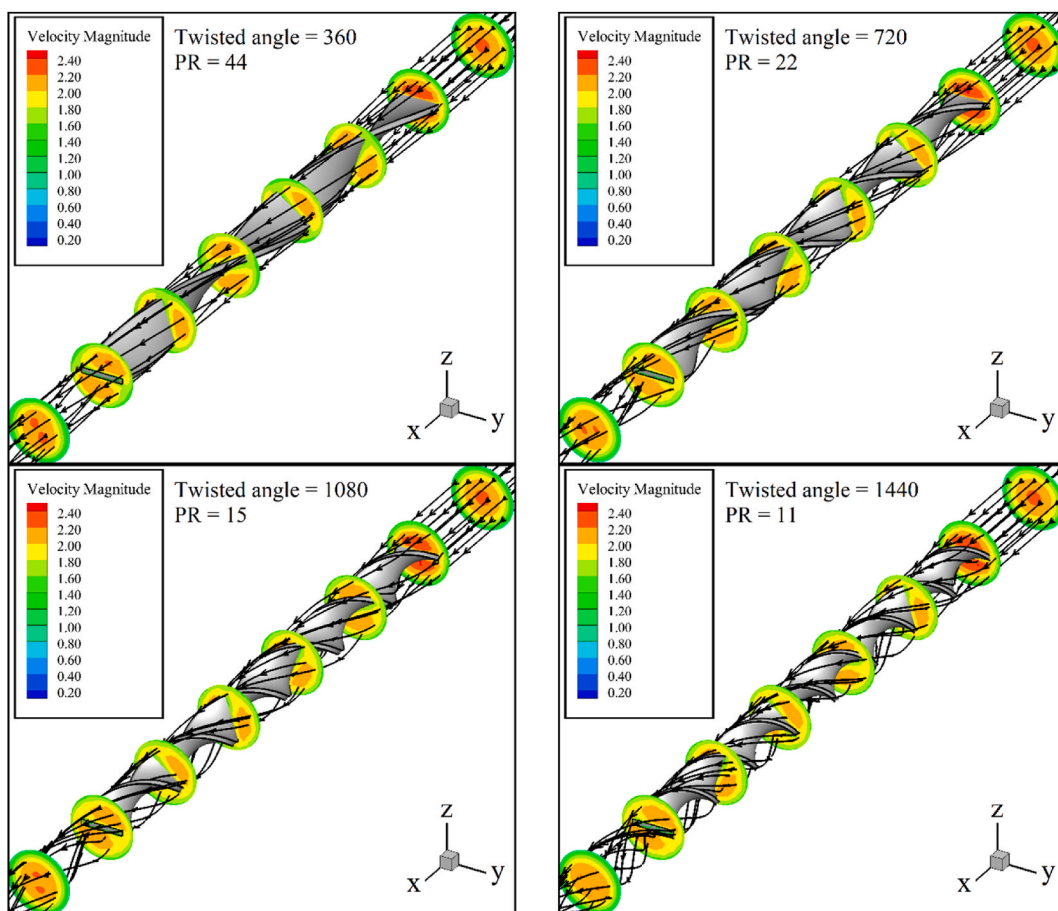

Fig. 7. The streamlines and the contours of velocity magnitude of tubes fitted with Case A turbulators (the values are in m/s).

5.3. The impact of the turbulators on the f values

The impacts of nanofluid fraction, *Re,* and *PR* on the *f* and *f/f₀* ratios are shown in Fig. 6. According to the results, the insertion of turbulators inside the tube increases the *f* dramatically compared to that of the simple tube (Fig. 4b), so that the maximum *f/f₀* ratios at Re = 4000, 6000, and 8000, are 6.300, 4.810, 4.481, respectively, which all belong to the tube with Case C turbulator and *PR* = 11. These values are significant, as they suggest that even though the *Nu* number was only increased up to 65.1 %, the *f* values were increased up to more than six times. The rise of the *f* value is associated with considerably higher pumping power, so not only does it lead to higher power consumption, but sometimes it requires more expensive and bigger pumping systems, which can create considerable problems in practice. This indicates that the trade-off between the increased *Nu* number and the raised *f* values should be examined more closely using the *PEC* to ensure that the presence of TT can be advantageous.

Considering the absolute values in these plots, it is apparent that raising the number of TT blades increases the contact surface with fluids, leading to higher *f* values. On the other hand, as the *PR* values are reduced, the twist angle of the TT is increased, raising the contact surface with the fluid and creating more complexity within the fluid flow. The changes in these values stem from alternating fluid flow behavior within the tubes. The turbulators lead to variation in the flow field which will be later discussed with streamlines. Aside from this, the velocity vector alters from the axial vector in the tube without the turbulator to two components of velocity in the tube with a turbulator which are named axial velocity and angular velocity. The changes in the velocity field are caused by the twisted geometry of the TTs and the fact that they can act as obstacles preventing the fluid flow from passing normally within the tube, which leads to the increase in the *f*. As can be observed, the influence of Re and *PR* parameters on the *f* values seems less complicated than their influence on the *Nu*. As the twist angle of the turbulator increases, which is associated with the decrease in *PR*, the TT blades act as a more intense obstacle in the axial direction of the fluid flow passage, which results in higher *f* values. Moreover, it is noticeable that raising the Re values reduces the friction factor, which is in line with the equation of this parameter, which has a fluid velocity value in its denominator. Also, raising the nanofluid concentration can increase the *f* value since it leads to higher fluid viscosity which is associated with higher pumping powers.
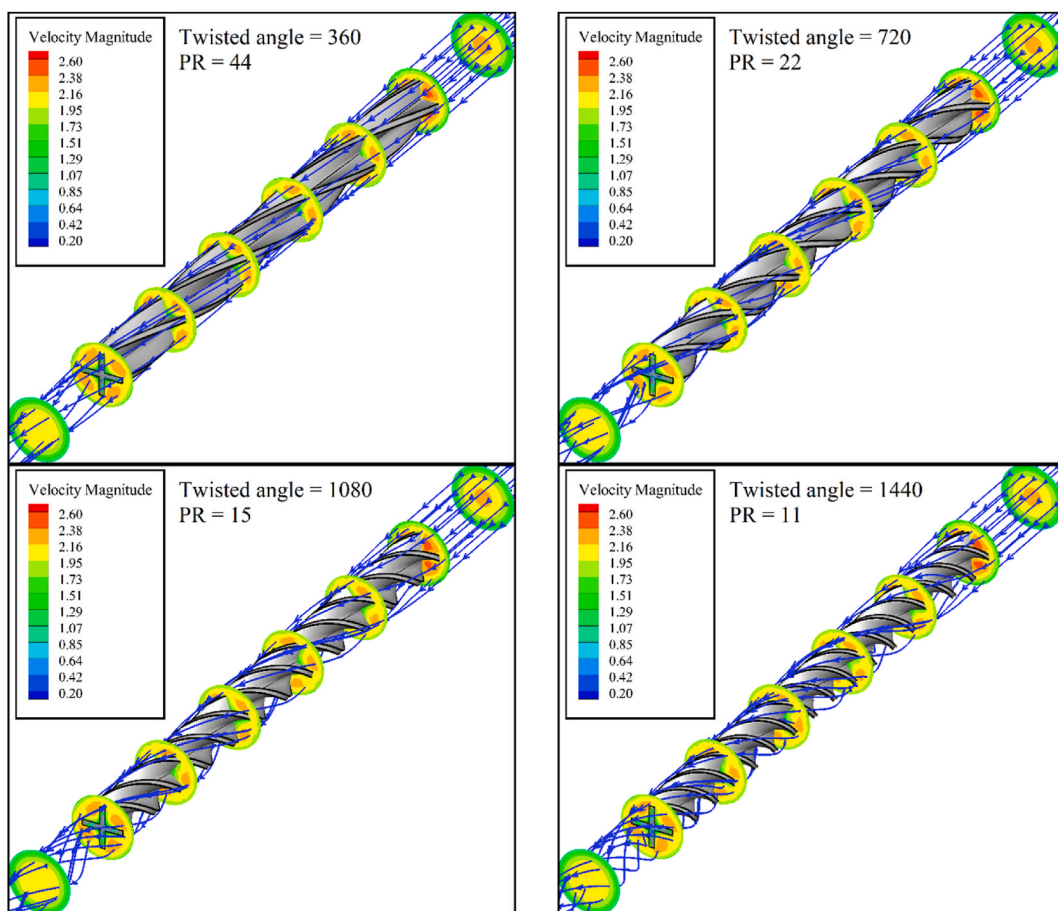

Fig. 8. The streamlines and the contours of velocity magnitude of tubes fitted with Case B turbulators (the values are in m/s).

5.4. The impact of turbulators on flow behavior and velocity contours

To analyze the changes in the flow pattern, it is necessary to examine velocity magnitude contours as well as streamlines. Fig. 7 illustrates the streamlines and velocity magnitude contours at various cross sections in the tube with Case A turbulator with different *PR* values of *PR* = 44, *PR* = 22, *PR* = 15, and *PR* = 11 at Re = 6000. It can be found that fluid flow behavior is altered by locating turbulators in the tube. The TT causes the fluid to revolve around the tube's axis, leading to the variation in the boundary layers on the heated wall. By inserting turbulators, the maximum velocity of the fluid at flow cross-sections does not occur in the center of the tube, and the velocity magnitude patterns undergo severe changes. Also, the fluid flow is forced to follow the rotational profile of the TTs, which is more significant when TTs have lower *PR* values (higher twist angles). In other words, the flow is more rotational with lower *PR* values.

Similarly, the streamlines and velocity magnitudes in the tube with the Case B turbulators are shown in Fig. 8. The velocity contours and streamlines are obtained for *PR* = 44, *PR* = 22, *PR* = 15, and *PR* = 11, at Re = 6000. Comparison between Figs. 6 and 7 suggests that the maximum fluid velocity at different cross sections increases by inserting the Case B turbulator instead of the Case A turbulator. By making use of the Case B turbulator, the flow passage area is decreased, which can increase the fluid velocity up to some extent for a constant mass flow rate. On the other hand, the contact surface between the fluid and turbulator is elevated in Case B, which can create the boundary layer on a wider surface (with no-slip boundary condition). Because the mass flow rate should remain constant, the reduction of fluid velocity in the vicinity of the wider boundary layer should be compensated by increasing the fluid velocity in the areas farther from the surface. Hence, the maximum velocity of the fluid in the tube with the Case B turbulator is more than that with the Case A turbulator.

Fig. 9 shows the velocity contours at different flow cross sections as well as streamlines in the tube with Case C turbulator. The results are achieved for different twist angles of the turbulator at Re = 6000. It can be found that the maximum velocity of the fluid at different flow cross sections for Case C is higher than those of Case B (Fig. 8) and Case A (Fig. 7). The contact surface between the fluid and the turbulator increases in Case C compared to those of Case B and Case A, which leads to the formation of the boundary layer on a wider region. The reduction of fluid velocity in the boundary layer occurs on the larger area which brings about the increase in the value of fluid velocity at sufficient distance from surfaces for having a constant mass flow rate of nanofluid.

Another point that can be considered important is that by increasing the twist angle, the fluid cannot completely flow through the grooves. The behavior of streamlines in the areas far away from the center of the tube reveals that the rotational motion of the fluid is not entirely consistent with the twist pattern of the turbulators. It means that the increase in the twist angle of tapes does not necessarily lead to the further rotational motion of fluid around the walls.

5.5. The impacts of the turbulators on the PEC values

Fig. 10 shows the effects of nanofluid concentration and *PR* on the *PEC* of heat exchangers with the turbulators of Case A, Case B, and Case C at various Re values. Based on the results, the maximum *PEC* values at Re = 4000, 6000, and 8000, were found to be 1.063, 1.052, and 1.032. On the other hand, the minimum *PEC* values at these Re numbers were calculated to be 0.881, 0.903, and 0.901. It is also noteworthy that at Re = 4000 and 6000, out of the 48 examined simulations conducted at each of these Re numbers, only 12 led to *PEC* values over 1 (25 % of cases). At Re = 8000, the results were even more frustrating, as only 11 cases had *PEC* values over 1 (22.9 % of the cases).

It is observed that the *PEC* value slightly decreases with the growth in the number of turbulator blades because as the number of blades is increased, the *f* values are increased so severely that cannot be compensated by the rise of the *Nu* number, which leads to considerably lower *PEC* values. Thus, the comparison between the acquired numerical results by employing the suggested cases in this article reveals that Case A has a more appropriate *PEC*. It is significant to note that the use of a turbulator with a higher number of blades, which leads to stronger rotational motion of fluid, does not necessarily increase the *PEC* value. Increasing *PR* is equivalent to decreasing the rotational angle of the turbulator. It was expected from most of the previous works that the higher values of the rotational angle of the TTs lead to the improvement of the *PEC* of the heat exchanger. The acquired numerical result by applying the proposed turbulators in this study is opposite to what is expected from previous works. It is shown that increasing the twist angle of the proposed turbulators reduces the *PEC* of the heat exchanger, which is more noticeable in the higher values of *Re*.

6. Conclusion

In this research, it was tried to find the possible adverse effects of using turbulators in tubular heat exchangers. The Nusselt number (*Nu*), friction factor (*f*), and the performance evaluation criterion (*PEC*) were used as decisive parameters. Also, streamlines and velocity magnitude contours were employed to examine the behavior of the fluid flow. For this purpose, several parametric studies including 156 cases with and without turbulators with different blades (Case A = 1, Case B = 2, and Case C = 3) and pitch ratios (*PR* = 44, 22, 15, and 11, equivalent to the twist angles of 2π, 4π, 6π and 8π, respectively) were examined at various Reynolds numbers (Re = 4000, 6000, and 8000) and titania nanoparticle concentrations (φ = 0.01, 0.02, and 0.03). The main findings are summarized as follows.

- Increasing the number of turbulator blades leads to higher *Nu* numbers. Based on the results, the Case C turbulator with three blades raised the *Nu* number by up to 65.1 %, 56.2 %, and 53.0 % compared to the benchmark cases, at Re = 4000, 6000, and 8000, respectively.
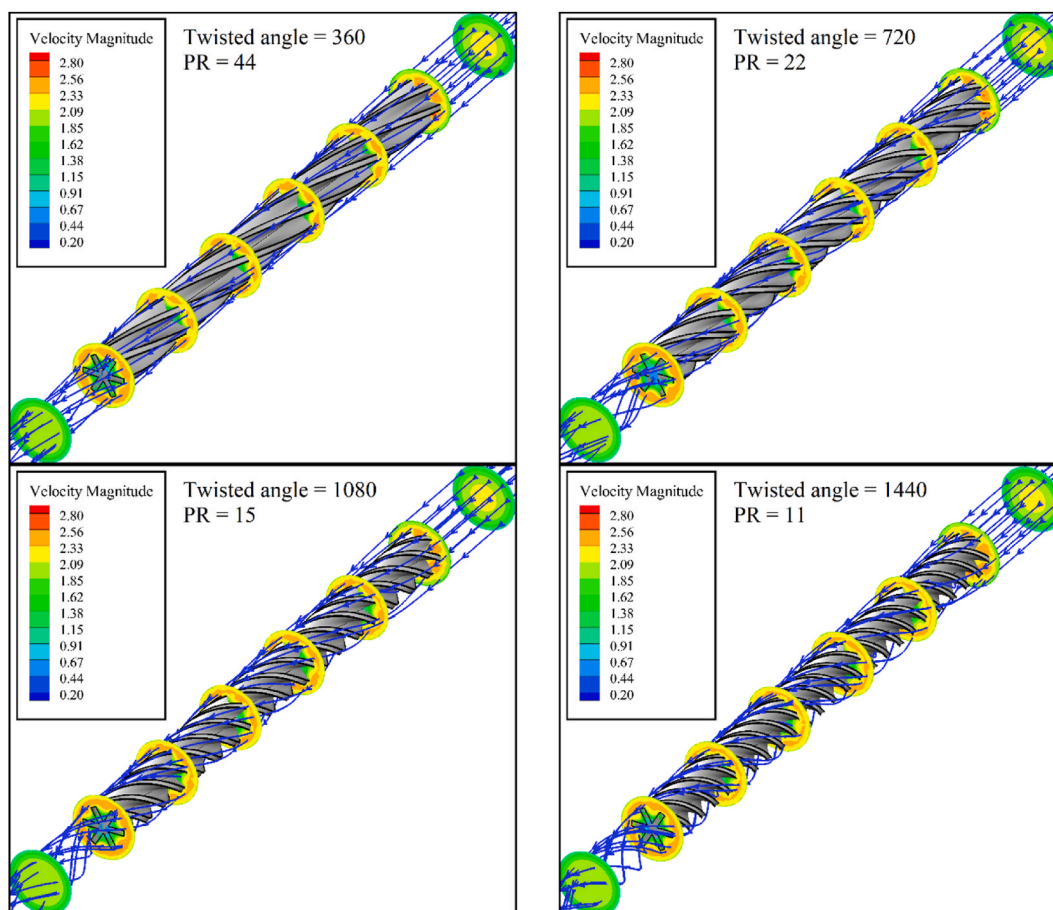
Fig. 9. The streamlines and the contours of velocity magnitude of tubes fitted with Case C turbulators (the values are in m/s).

- The *Nu* number has a negative relationship with the *PR* at Re = 4000 and a positive relationship at Re = 8000. At Re = 6000, the connection between these two parameters is more complex as it depends on the case and nanoparticle concentration.
- The *f* is significantly raised by inserting turbulators, and the influence of these devices is more considerable on this parameter than on the *Nu* number.
- A higher number of blades and lower *PR* values lead to higher *f* values, so that the f/f_0 for the case with Case C turbulator and *PR* = 11 was 6.300, meaning that the friction factor was raised by up to more than six times.
- Lower number of turbulator blades, and higher *PR* values provide better *PEC* values (Case A turbulator with *PR* = 44), even though the provided improvement is limited to only 6.3 %.
- In 25 %, 25 %, and 22.9 % of the examined cases with Case A, Case B, and Case C turbulators, the *PEC* value was dropped to lower than 1, meaning that the overall performance of the heat exchanger was reduced in the majority of examined cases.
- While with the best turbulator, the *PEC* value was increased by only 6.3 %, some of the turbulators reduced this parameter by up to 11.8 %, which is more severe.
- Employing turbulators is suggested as one of the solutions that, if used properly, can increase the heat exchanger efficiency. This study reveals that heat transfer and PEC do not necessarily improve by applying turbulators.

It is recommended that researchers in this field focus on adding some minor alternations to traditional TT inserts instead of working on multi-bladed ones which are associated with considerable pressure drops.

Data availability

The data that support the findings of this research are available from the corresponding author upon reasonable request.

CRediT authorship contribution statement

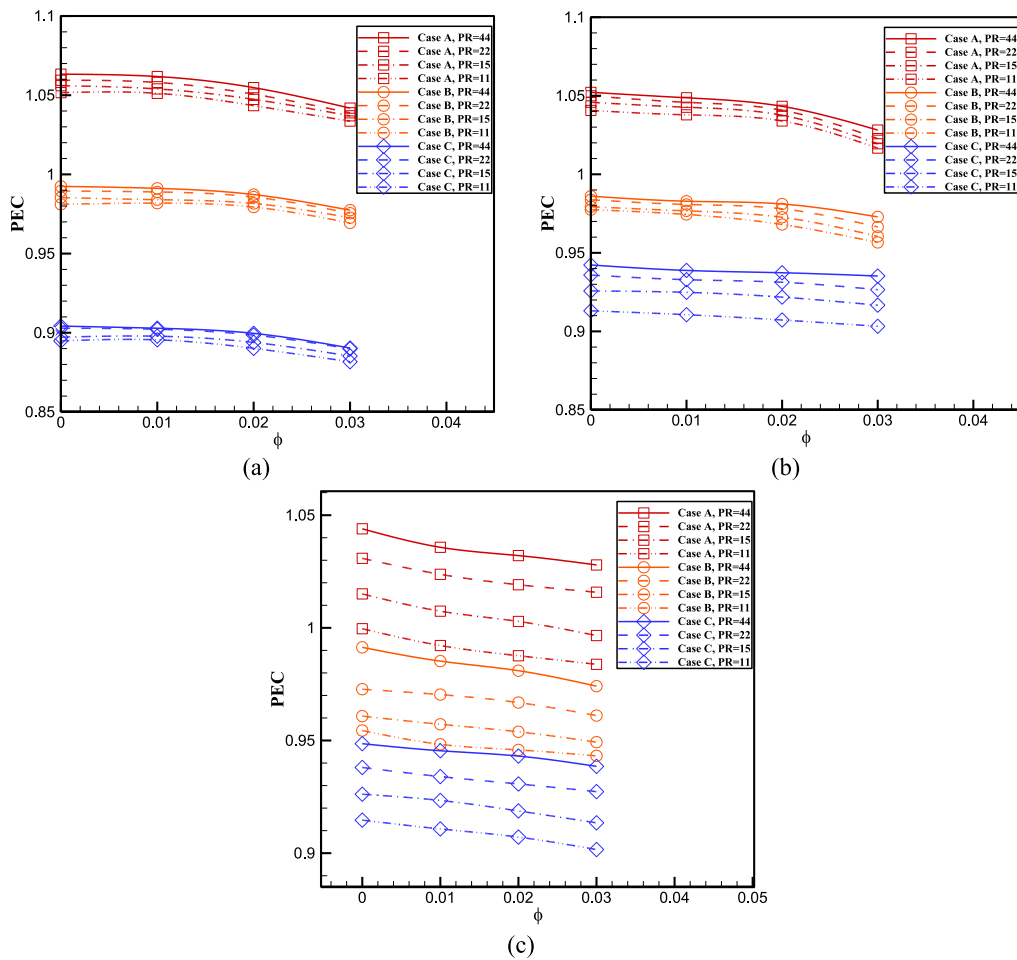**Ali Mohadjer:** Writing – original draft, Visualization, Software, Methodology, Investigation, Conceptualization. **Mohammad**

Fig. 10. Variation of *PEC* for different PRs at (a) Re = 4000, (b) Re = 6000, and (c) Re = 8000.

Hasan Nobakhti: Writing – review & editing, Writing – original draft, Supervision, Project administration, Investigation, Formal analysis, Data curation. **Alireza Nezamabadi:** Writing – review & editing, Supervision, Resources, Data curation. **Seyed Soheil Mousavi Ajarostaghi:** Writing – review & editing, Validation, Software, Resources, Project administration, Methodology.

Declaration of competing interest

The authors declare that they have no known competing financial interests or personal relationships that could have appeared to influence the work reported in this paper.

References

[1] D. D'Agostino, S. Mazzella, F. Minelli, F. Minichiello, Obtaining the NZEB target by using photovoltaic systems on the roof for multi-storey buildings, Energy Build. 267 (2022) 112147, https://doi.org/10.1016/j.enbuild.2022.112147.

[2] F. Minelli, D. D'Agostino, M. Migliozzi, F. Minichiello, P. D'Agostino, *PhloVer: a Modular and integrated tracking photovoltaic shading Device for sustainable large urban spaces—preliminary Study and prototyping.* Energies 16 (15) (2023) 5786.

[3] H.A. Amiri, F. Afsharpanah, S. Moshafi, S. Asiaei, Thermal management of an asymmetrical wavy microchannel heat sink via Ag/water nanofluid, Case Stud. Therm. Eng. 53 (2024) 103857, https://doi.org/10.1016/j.csite.2023.103857.

[4] M. Sheikholeslami, M. Jafaryar, M. Barzegar Gerdroodbary, A.H. Alavi, Influence of novel turbulator on efficiency of solar collector system, Environ. Technol. Innovat. 26 (2022) 102383, https://doi.org/10.1016/j.eti.2022.102383.

[5] F. Afsharpanah, S.S. Mousavi Ajarostaghi, M. Arıcı, Parametric study of phase change time reduction in a shell-and-tube ice storage system with anchor-type fin design, Int. Commun. Heat Mass Tran. 137 (2022) 106281, https://doi.org/10.1016/j.icheatmasstransfer.2022.106281.

[6] F. Afsharpanah, K. Pakzad, S.S. Mousavi Ajarostaghi, M. Arıcı, Assessment of the charging performance in a cold thermal energy storage container with two rows of serpentine tubes and extended surfaces, J. Energy Storage 51 (2022) 104464, https://doi.org/10.1016/j.est.2022.104464.

[7] F. Afsharpanah, K. Pakzad, S.S. Mousavi Ajarostaghi, S. Poncet, K. Sedighi, Accelerating the charging process in a shell and dual coil ice storage unit equipped with connecting plates, Int. J. Energy Res. 46 (6) (2022) 7460–7478, https://doi.org/10.1002/er.7654.

[8] J. Luo, A. Alghamdi, F. Aldawi, H. Moria, A. Mouldi, H. Loukil, A.F. Deifalla, S.P. Ghoushchi, Thermal-frictional behavior of new special shape twisted tape and helical coiled wire turbulators in engine heat exchangers system, Case Stud. Therm. Eng. 53 (2024) 103877, https://doi.org/10.1016/j.csite.2023.103877.

[9] A. Boonloi, N. Lewpiriyawong, W. Jedsadaratanachai, Performance improvement in a heat exchanger tube using discrete X–V baffle (DXVB) turbulators, Case Stud. Therm. Eng. (2024) 103999, https://doi.org/10.1016/j.csite.2024.103999.

[10] G. Ashraf, S. Bilal, M. Ishaq, S. Khalid Saifullah, A.S. Alqahtani, M.Y. Malik, Thermodynamic optimization in laminar and fully developed flow in double pipe heat exchanger with arrow-shaped extended surfaces: a novel design, Case Stud. Therm. Eng. 54 (2024) 103947, https://doi.org/10.1016/j.csite.2023.103947.

[11] P.M.J. Stalin, R. Lokanadham, G. Naveen, B. Singh, S.A. Tayyab, H. Panchal, A. Kumar, M.I.H. Siddiqui, L. Natrayan, M.A. Shah, Innovative cinque rib-roughened stimulators on performance improvement in triangular channel solar air heater, Int. J. Low Carbon Technol. 19 (2024) 227–235, https://doi.org/10.1093/ijlct/ctae002.

[12] H. Singh, T. Alam, M.I. Haque Siddiqui, M. Ashraf Ali, D. Sagar, Experimental investigation of heat transfer augmentation due to obstacles mounted in solar air heater duct, Exp. Heat Tran. 37 (2) (2024) 162–181, https://doi.org/10.1080/08916152.2022.2108166.

[13] T. Alam, M.I.H. Siddiqui, H. Alshehri, M.A. Ali, P. Blecich, K. Saurabh, *Exergy-based thermo-hydraulic Performance of roughened Absorber in solar air heater duct.* Applied sciences 12 (3) (2022) 1696.

[14] A. Kumar, R. Kunwer, R.K. Donga, S. Kumar Priyanka, T. Alam, M.I.H. Siddiqui, D. Dobrotă, Effect of oval rib parameters on heat transfer enhancement of TiO2/water nanofluid flow through parabolic trough collector, Case Stud. Therm. Eng. 55 (2024) 104080, https://doi.org/10.1016/j.csite.2024.104080.

[15] A.P. Dash, T. Alam, M.I.H. Siddiqui, P. Blecich, M. Kumar, N.K. Gupta, M.A. Ali, A.S. Yadav, *Impact on heat transfer rate due to an extended surface on the passage of microchannel using cylindrical ribs with varying sector angle, Energies 15 (21) (2022) 8191.*

[16] S. Ishaque, M.I.H. Siddiqui, M.-H. Kim, Effect of heat exchanger design on seasonal performance of heat pump systems, Int. J. Heat Mass Tran. 151 (2020) 119404, https://doi.org/10.1016/j.ijheatmasstransfer.2020.119404.

[17] M. Shahzad Nazir, A. Shahsavar, M. Afrand, M. Arıcı, S. Nižetić, Z. Ma, H.F. Öztop, A comprehensive review of parabolic trough solar collectors equipped with turbulators and numerical evaluation of hydrothermal performance of a novel model, Sustain. Energy Technol. Assessments 45 (2021) 101103, https://doi.org/10.1016/j.seta.2021.101103.

[18] S. Chupradit, A.T. Jalil, Y. Enina, D.A. Neganov, M.S. Alhassan, S. Aravindhan, A. Davarpanah, Use of organic and copper-based nanoparticles on the turbulator installment in a shell tube heat exchanger: a CFD-based simulation approach by using nanofluids, J. Nanomater. 2021 (2021) 3250058, https://doi.org/10.1155/2021/3250058.

[19] Z. Esmaeili, S. Akbarzadeh, S. Rashidi, M.S. Valipour, Effects of hybrid nanofluids and turbulator on efficiency improvement of parabolic trough solar collectors, Eng. Anal. Bound. Elem. 148 (2023) 114–125, https://doi.org/10.1016/j.enganabound.2022.12.024.

[20] Q. Xiong, M. Izadi M, Shokri rad, S.A. Shehzad, and H.A. Mohammed, *3D numerical Study of Conical and fusiform Turbulators for heat transfer Improvement in a double-pipe heat exchanger*, Int. J. Heat Mass Tran. 170 (2021) 120995, https://doi.org/10.1016/j.ijheatmasstransfer.2021.120995.

[21] P.K. Chaurasiya, S.K. Singh, P.K. Jain, U. Rajak, T.N. Verma, A.K. Azad, K. Choudhary, A.M. Alosaimi, A. Khan, Heat transfer and friction factor correlations for double pipe heat exchanger with inner and outer corrugation, Energy Sources, Part A Recovery, Util. Environ. Eff. 45 (1) (2023) 18–45, https://doi.org/10.1080/15567036.2021.1953635.

[22] M. Jafaryar, M. Sheikholeslami, Z. Li, *CuO-water nanofluid flow and heat transfer in a heat exchanger tube with twisted tape turbulator.* Powder technology 336 (2018) 131–143.

[23] M. Sheikholeslami, M. Jafaryar, Z. Li, Second law analysis for nanofluid turbulent flow inside a circular duct in presence of twisted tape turbulators, J. Mol. Liq. 263 (2018) 489–500.

[24] M. Ghasemian, M. Sheikholeslami, M. Dehghan, Performance improvement of photovoltaic/thermal systems by using twisted tapes in the coolant tubes with different cross-section patterns, Energy 279 (2023) 128016, https://doi.org/10.1016/j.energy.2023.128016.

[25] J. Heeraman, R. Kumar, P.K. Chaurasiya, H. Ivanov Beloev, I. Krastev Iliev, Experimental evaluation and thermal performance analysis of a twisted tape with dimple configuration in a heat exchanger, Case Stud. Therm. Eng. 46 (2023) 103003, https://doi.org/10.1016/j.csite.2023.103003.

[26] S.K. Singh, R. Kacker, P.K. Chaurasiya, S.S. Gautam, Correlations on heat transfer rate and friction factor of a rectangular toothed v-cut twisted tape exhibiting the combined effects of primary and secondary vortex flows, Int. Commun. Heat Mass Tran. 139 (2022) 106503, https://doi.org/10.1016/j.icheatmasstransfer.2022.106503.

[27] L. Syam Sundar, Heat transfer, friction factor and exergy efficiency analysis of nanodiamond-Fe3O4/water hybrid nanofluids in a tube with twisted tape inserts, Ain Shams Eng. J. 14 (9) (2023) 102068, https://doi.org/10.1016/j.asej.2022.102068.

[28] B. Samutpraphut, S. Eiamsa-ard, V. Chuwattanakul, C. Thianpong, N. Maruyama, M. Hirota, Influence of sawtooth twisted tape on thermal enhancement of heat exchanger tube, Energy Rep. 9 (2023) 696–703, https://doi.org/10.1016/j.egyr.2022.11.029.

[29] Z. Feng, Z. Li, Z. Hu, Y. Lan, S. Zheng, Q. Zhang, J. Zhou, J. Zhang, Combined influence of rectangular wire coil and twisted tape on flow and heat transfer characteristics in square mini-channels, Int. J. Heat Mass Tran. 205 (2023) 123866, https://doi.org/10.1016/j.ijheatmasstransfer.2023.123866.

[30] M. Noorbakhsh, S.S.M. Ajarostaghi, M. Zaboli, B. Kiani, Thermal analysis of nanofluids flow in a double pipe heat exchanger with twisted tapes insert in both sides. Journal of Thermal Analysis and Calorimetry 147 (5) (2022) 3965–3976, https://doi.org/10.1007/s10973-021-10738-x.

[31] Z. Said, M.A. Sabiha, R. Saidur, A. Hepbasli, N.A. Rahim, S. Mekhilef, T.A. Ward, Performance enhancement of a flat plate solar collector using titanium dioxide nanofluid and polyethylene glycol dispersant, J. Clean. Prod. 92 (2015) 343–353, https://doi.org/10.1016/j.jclepro.2015.01.007.

[32] A.A. Sedighi, M. Bazargan, *A CFD analysis of the pollutant dispersion from cooling towers with various configurations in the lower region of atmospheric boundary layer.* Science of the Total Environment 696 (2019) 133939.

[33] A.A. Sedighi, Z. Deldoost, B.M. Karambasti, Effect of thermal energy storage layer porosity on performance of solar chimney power plant considering turbine pressure drop, Energy 194 (2020) 116859.

[34] A.A. Sedighi, Z. Deldoost, M. Bazargan, Desirable effects of cutting grooves on inner side of small cooling tower on reduction in ground level pollutant concentration. Journal of the Brazilian Society of Mechanical Sciences and Engineering 42 (235) (2020) 235.

[35] M. Zaboli, M. Nourbakhsh, S.S.M. Ajarostaghi, Numerical evaluation of the heat transfer and fluid flow in a corrugated coil tube with lobe-shaped cross-section and two types of spiral twisted tape as swirl generator. Journal of Thermal Analysis and Calorimetry 147 (1) (2022) 999–1015, https://doi.org/10.1007/s10973-020-10219-7.

[36] Y. Hong, X. Deng, L. Zhang, 3D numerical Study on compound heat transfer Enhancement of converging-diverging tubes Equipped with twin twisted Tapes, J. Chem. Eng. 20 (3) (2012) 589–601, https://doi.org/10.1016/S1004-9541(11)60223-1. Chinese.

[37] L.B. Ramoul, A. Korichi, C. Popa, H. Zaidi, G. Polidori, Numerical study of flow characteristics and pollutant dispersion using three RANS turbulence closure models, Environ. Fluid Mech. 19 (2) (2019) 379–400.

[38] B.M. Karambasti, A.A. Sedighi, Numerical investigation of flow and heat transfer of Al2O3-water nanofluid in a channel partially filled with porous media considering effects of temperature on the properties of nanofluid. Advanced science, Eng. Med. 11 (9) (2019) 817–822.

[39] M. Corcione, Empirical correlating equations for predicting the effective thermal conductivity and dynamic viscosity of nanofluids. Energy conversion and management 52 (1) (2011) 789–793.

[40] F. Afsharpanah, S.S. Mousavi Ajarostaghi, F. Akbarzadeh Hamedani, M. Saffari Pour, Compound heat transfer augmentation of a shell-and-coil ice storage unit with metal-oxide nano additives and connecting plates, Nanomaterials 12 (6) (2022) 1010.

[41] S. Eiamsa-ard, P. Promvonge, Thermal characteristics in round tube fitted with serrated twisted tape, Appl. Therm. Eng. 30 (13) (2010) 1673–1682, https://doi.org/10.1016/j.applthermaleng.2010.03.026.